Finite-temperature dynamical quantum phase transition in a non-Hermitian system

Debashish Mondal [1,2,*] and Tanay Nag [3,†]

[1]*Institute of Physics, Sachivalaya Marg, Bhubaneswar-751005, India*

[2]*Homi Bhabha National Institute, Training School Complex, Anushakti Nagar, Mumbai 400094, India*

[3]*Department of Physics and Astronomy, Uppsala University, Box 516, 75120 Uppsala, Sweden*

(Received 4 January 2023; revised 10 April 2023; accepted 12 May 2023; published 24 May 2023)

We investigate the interplay between non-Hermiticity and finite temperature in the context of a mixed-state dynamical quantum phase transition (MSDQPT). We consider a *p*-wave superconductor model, encompassing complex hopping and non-Hermiticity, that can lead to gapless phases in addition to gapped phases, to examine the MSDQPT and winding number via the intraphase quench. We find that the MSDQPT is always present irrespective of the gap structure of the underlying phase; however, the profile of Fisher zeros changes between the above phases. Such occurrences of MSDQPT are in contrast to the zero-temperature case in which a DQPT does not take place for the gapped phase. Surprisingly, the half-integer jumps in winding number at zero temperature are washed away for finite temperature in the gapless phase. We study the evolution of the minimum time required by the system to experience MSDQPT with the inverse temperature such that gapped and gapless phases can be differentiated. Our study indicates that the minimum time shows monotonic (nonmonotonic) behavior for the gapped (gapless) phase.

DOI: 10.1103/PhysRevB.107.184311

I. INTRODUCTION

Equilibrium phase transitions are associated with the nonanalyticities in the free-energy density that are marked by the zeros of the partition function, namely Fisher zeros [1–3]. In the nonequilibrium case, the dynamical free-energy density becomes singular at certain critical times in the complex time plane where the dynamical quantum phase transitions (DQPTs) take place [4–14]. When the time-evolved state under a sudden quench is orthogonal to the initial state, the DQPTs occur corresponding to the vanishing Loschmidt amplitude (LA) [15–21]; this refers to the dynamical analogs of equilibrium quantum phase transitions at quantum critical points (QCPs). It has been shown that one can observe a DQPT even without quenching across the QCPs in sudden quench [12,22–31]. This list extends further to slow quenches [32–35], Floquet driving [36–41], interacting systems [24,42–44], bosonic systems [45–47], time crystals [48,49], etc.

Thanks to the open quantum systems [50,51] and quasiparticle systems with a finite lifetime [52–54], the Hermitian description of the problem expands to the non-Hermitian realm where exceptional points (EPs) appear instead of QCPs [54–61]. As a result, the dynamical order parameter, namely the winding number [13,62], characterizing the topological properties of the real-time dynamics can show an intriguing jump profile as far as the nonunitary evolution of the non-Hermitian is concerned [63–67]. The DQPTs are experimentally observed in trapped-ion [68], nuclear magnetic resonance [69], optical lattice [70] systems. On the other hand, the non-Hermitian effects are practically realized in metamaterials such as cold-atom [71,72], photonic [73,74], and acoustic [75,76] systems. Hence, it is important to study the interplay between a DQPT and non-Hermiticity from a theoretical as well as experimental point of view.

The finite-temperature extension of a QPT has recently been examined in the context of LA [77–80]. Following a similar line of argument, the DQPT is investigated following an initial thermal distribution instead of a pure quantum state [10,28,81–85]. This brings in the concept of density matrix, characterized by an inverse temperature, leading to the mixed-state DQPT (MSDQPT) where the quantum coherence is lost. For the open quantum systems, contact with the thermal bath can potentially lead to such MSDQPT [64,86,87]. Given the fact that the DQPT persists in finite temperature [10,64] and it can show an anomaly in the non-Hermitian system [67], we pose here the following intriguing questions to understand the interplay between the non-Hermiticity and finite temperature: Can MSDQPT appear (disappear) when the DQPT in the underlying non-Hermitian system at zero temperature is absent (present)? Can we differentiate various non-Hermitian phases by examining the MSDQPT? How do we understand the topology in the real-time dynamics of the non-Hermitian MSDQPT?

In this paper, we generalize the framework of the DQPT and the winding number for non-Hermitian finite-temperature cases such that the Hermitian and infinite-temperature limits can be successfully extracted. Considering a one-dimensional (1D) *p*-wave superconductor with complex hopping and non-Hermiticity (see Fig. 1), we find that sudden quench

*debashish.m@iopb.res.in

†tanay.nag@physics.uu.se

within the gapped phase exhibits MSDQPT, unlike the zero-temperature case [67] (see Fig. 2). Interestingly, we only observe integer jumps as a signature of MSDQPT for the sudden quenches within the gapless phases contrasting the zero-temperature profile of the DQPT as observed previously (see Figs. 3 and 4). However, the winding number shows nonmonotonic behavior in one of the gapless phases. The threshold time, referred to as the minimum critical time $t_{\rm cm}$, above which MSDQPT starts appearing, can be different from the zero- as well as infinite-temperature limit (see Fig. 5). We can distinguish various gapless and gapped phases by investigating the behavior of $t_{\rm cm}$ with temperature. The above studies on lossy superconductivity are further extended to the lossy chemical potential case for completeness. Our study thus indicates that the temperature can nontrivially modify the dynamics of EPs, as evident from the emergence of MSDQPT.

The structure of this paper is the following. We present the framework of MSDQPT in Sec. II for finite temperature and non-Hermiticity. Next, we demonstrate the model under consideration in Sec. III. We examine the MSDQPT results for a gapped phase in Sec. IV A and for gapless phases in Secs. IV B and IV C. We differentiate among these phases with respect to their temperature profile in Sec. IV D. We provide a plausible explanation behind our findings in Sec. IV E. Finally, we conclude in Sec. V.

II. MSDQPT FRAMEWORK

Let us consider a two-level system, described by the Hamiltonian $H_k = \mathbf{h}_k \cdot \boldsymbol{\sigma} = h_k \hat{h}_k \cdot \vec{\sigma}$, that is thermally attached to a heat bath at temperature $T = 1/\beta$; here $\mathbf{h}_k = \{h_k^x, h_k^y, h_k^z\}$ and $\boldsymbol{\sigma} = \{\sigma_x, \sigma_y, \sigma_z\}$. Note that H_k can be considered to be non-Hermitian without loss of generality where h_k^i can be complex with $i = x, y, z$. The associated density matrix takes the form $\rho_k = \exp(-\beta H_k)/\operatorname{Tr}[\exp(-\beta H_k)] = \sigma_0 - m(\hat{h}_k \cdot \vec{\sigma})/2$, where $m = \tanh(\beta h_k)$ (see Appendix A for more details). We start with this finite-temperature initial mixed state at time $t = 0$, i.e., $\rho_k(0)$ corresponding to $H_{k,i}$, and suddenly quench to the final Hamiltonian $H_{k,f}$ such that the LA at a later time t is given by [10] $g_k(t) = \operatorname{Tr}[\rho_k(0)U_k(t)] = \cos(h_{k,f}t) - i\ \sin(h_{k,f}t)B_k$ with $U_k(t) = e^{-iH_{k,f}t}$ and $B_k = -m(\vec{h}_{k,i} \cdot \vec{h}_{k,f}/h_{k,i}h_{k,f})$ (see Appendix B for more details). The dynamical analog of free energy is called the rate function, which is given by the logarithm of LA [62],

$$I(t) = -\frac{1}{2\pi}\int_{\rm BZ} \ln(|g_k(t)|^2). \tag{1}$$

The nonanalyticities in the rate function, given by $g_k(t) = 0$, cause the Fisher zeros to appear in the complex time plane (see Appendix C for more details)

$$z_{n,k} = i\left(n + \frac{1}{2}\right)\frac{\pi}{h_{k,f}} + \frac{1}{h_{k,f}}\tanh^{-1}(B_k), \tag{2}$$

where $z_{n,k} = it$ and $n \in Z$. Note that the zeros of the partition function are referred to as Fisher zeros. As a result, MSDQPT occurs at the momentum $k = k_c$ and critical time $t_c = -iz_{n,k_c}$ where $\operatorname{Re}[z_{n,k_c}] = 0$, leading to

$$\pi(n + 1/2)\operatorname{Im}\left[h_{k_c,f}\right] + \operatorname{Re}\left[h_{k_c,f}\right]\operatorname{Re}\left[C_{k_c}\right] + \operatorname{Im}\left[h_{k_c,f}\right]\operatorname{Im}\left[C_{k_c}\right] = 0 \tag{3}$$

and

$$t_c = \pi\left(n + \frac{1}{2}\right)\frac{\operatorname{Re}\left[h_{k_c,f}\right]}{\left|h_{k_c,f}\right|^2} + \frac{\operatorname{Re}\left[h_{k_c,f}\right]\operatorname{Im}\left[C_{k_c}\right] - \operatorname{Im}\left[h_{k_c,f}\right]\operatorname{Re}\left[C_{k_c}\right]}{\left|h_{k_c,f}\right|^2} \tag{4}$$

with $C_k = \tanh^{-1}(B_k)$ (see Appendixes D and E for more details). To be precise, MSDQPT occurs when z_n, k crosses the positive side of the imaginary axis such that positive t_c's can only be the meaningful solutions of Eq. (4).

On the other hand, the dynamical phase is given by (see Appendix F for more details)

$$\Phi_k^{\rm dyn}(t) = -\int_0^t dt' \operatorname{Re}\left[h_{k,f}\frac{\tanh(2\operatorname{Im}[h_{k,f}]\,t') - m}{1 - m\,\tanh(2\operatorname{Im}[h_{k,f}]\,t')}\right]. \tag{5}$$

The winding number, capturing the dynamical order parameter [88], appears to be

$$\nu(t) = \oint_{\rm BZ} dk\,\frac{\partial \Phi_k^G(t)}{\partial k}, \tag{6}$$

with $\Phi_k^G(t) = \Phi_k^{\rm tot}(t) - \Phi_k^{\rm dyn}(t)$ and $\Phi_k^{\rm tot}(t) = -\ln(\frac{g_k(t)}{|g_k(t)|})$. Hence the geometric phase is the net phase acquired by a nonequilibrium quantum system other than the dynamical phase.

The physical picture of MSDQPT refers to the quantum dynamics of a mixed-state density matrix. The MSDQPT essentially captures the interference between the time-evolved and initial density matrices. To be precise, where there is a complete destructive interference in real time, i.e., $g_k(t) = 0$, the rate function exhibits a singular behavior. Using the concept of parallel transport, it has been shown that noncyclic and unitary quantum evolutions of a pure quantum state are related to that of a mixed state [88]. Therefore, the geometric phases for a mixed state can be thoroughly investigated with real time following the analysis of MSDQPT. The non-Hermiticity can effectively mimic the effect of an external bath attached to a quantum system, and/or interaction in the quantum system. In the present context, our study qualitatively tracks the evolution of the geometric phase, associated with a mixed state, in an interacting system by considering a non-Hermitian system.

III. MODEL

We consider the non-Hermitian analog of a 1D p-wave superconductor with complex hopping as follows: $H(\gamma_1, \gamma_2, \phi) = \Sigma_k \psi_k \mathcal{H}_k(\gamma_1, \gamma_2, \phi)\psi_k^\dagger$ with Nambu basis $\psi_k = (c_k, c_{-k}^\dagger)$ [67,89–92],

$$\mathcal{H}_k(\gamma_1, \gamma_2, \phi) = 2w_0 \sin\phi \sin k\, I + \left(2\Delta \sin k + \frac{i\gamma_2}{2}\right)\sigma_y - \left(2w_0 \cos\phi \cos k + \mu + \frac{i\gamma_1}{2}\right)\sigma_z = \mathbf{h}_k \cdot \boldsymbol{\sigma}, \tag{7}$$

where w_0, $\phi \in [0, \pi/2]$, Δ, μ are the nearest-neighbor hopping amplitude, the hopping phase, the superconducting gap,

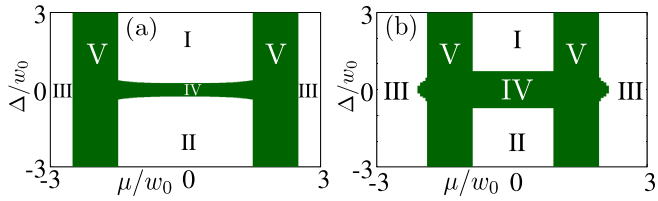

FIG. 1. The phase diagram of the model Hamiltonian $H(0, 1, 0)$ $[H(0, 1, \pi/4)]$, given by Eq. (7), is shown in (a) [(b)]. The white regions I, II, and III correspond to the gapped phase, while green regions IV and V denote the gapless phases. With increasing ϕ, phase IV increases in size while non-Hermiticity solely determines the width of phase V.

and the chemical potential, respectively. The non-Hermiticity in h_k^y for the p-wave superconductor gap function, referred to as the lossy superconductivity, might be caused by the spatially separated pairing processes [93]. On the other hand, the non-Hermiticity in h_k^z can be originated by the nonreciprocal hopping [94] or/and loss and gain in the chemical potential [95].

The Hamiltonian Eq. (7) becomes gapless for critical momentum k_* when the real part of the energies satisfies the following condition:

$$(2w_0 \cos\phi \cos k_* + \mu)^2 - \frac{\gamma_1^2}{4} + 4\Delta^2 \sin^2 k_* - \frac{\gamma_2^2}{4} = 4w_0^2 \sin^2\phi \sin^2 k_*. \tag{8}$$

This allows us to chart out the phases diagram of the model Hamiltonian as shown in Fig. 1. For $\gamma_1 = 0$ and $\gamma_2 \neq 0$, the gapless phase IV is bounded by horizontal lines $\Delta = \pm\sqrt{(4w_0^2 \sin^2\phi + \gamma_2^2/4 - \mu^2 \sin^2\phi)/(4 - \mu^2/w^2)}$ between the neighboring gapless phase V that are bounded by $[-2w_0 \cos\phi - \gamma_2/2, -2w_0 \cos\phi + \gamma_2/2]$ $([2w_0 \cos\phi - \gamma_2/2, 2w_0 \cos\phi + \gamma_2/2])$ in the left (right) side. Notice that gapless phase IV is primarily caused by the phase of the complex hopping, while the non-Hermiticity term γ_2 is solely responsible for the other gapless phase V. Phases I and II are topological, while phase III is trivial. Notice that for the calculation of the DQPT, we discard the identity term in Eq. (7) as it does not alter nonequilibrium evolution.

IV. RESULT

We focus on the gapped and gapless phases in the above model in the presence of lossy superconductivity only. The MSDQPT is studied for the intraphase quench. For completeness, we briefly discuss the fate of MSDQPT for other interphase quench. We also discuss the MSDQPT in the above model with a non-Hermitian chemical potential. The Hermitian counterpart of MSDQPT is demonstrated in Appendix I.

A. Quench within gapped phase I

We first examine the MSDQPT following the quench within phase I as shown in Fig. 1(b). For finite temperature ($\beta = 1$), the Fisher zeros profile, the rate function, the geometric phase, and the winding number are depicted in

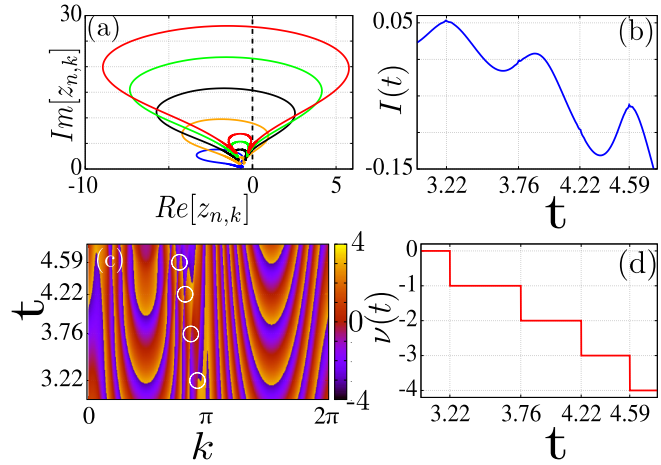

FIG. 2. We demonstrate (a) the lines of Fisher zeros $z_{n,k}$ with $n = 0$ (blue), …, $n = 4$ (red), as computed from Eq. (2); (b) nonanalytic nature in the rate function $I(t)$ as obtained from Eq. (1); (c) the geometric phase $\Phi_k^G(t)$ with time and momenta; and (d) the time evolution of winding number $\nu(t)$, quantified by Eq. (6) for the case discussed in Sec. IV A. The Fisher zeros $z_{n,k}$ cross an imaginary axis twice leading to the critical times $t_c \approx 3.22, 3.76, 4.22, 4.59, \ldots$, where $\nu(t)$ shows integer jumps. The white circles in (c) highlight the abrupt changes in the geometric phase. The parameters are taken to be $(\mu_i, \mu_f, \Delta_i, \Delta_f) = (0.1, 0.7, 2.2, 2.2)$. We consider $\beta = 1$, $w_0 = 1$, $\phi = \pi/4$, $\gamma_1 = 0$, and $\gamma_2 = 1$ for Figs. 2–4.

Figs. 2(a), 2(b), 2(c), and 2(d), respectively, referring to the fact that MSDQPT takes place. We notice that $z_{n,k}$ always cross the imaginary axis except for $n = n_{\min} = 0$. What we find is that $n_{\min}$ increases from zero as β increases, indicating the emergence of MSDQPT for any temperature. Interestingly, the nonanalyticities are not visible macroscopically; however, there exists the singular microstructures at a critical time $t = t_c \approx 3.22, 3.76, 4.22, 4.59, \ldots$ over the oscillating profile. We find abrupt changes in the geometric phase $\Phi_k^G(t)$, marked by white circles in Fig. 1(c), around the above values of t for k being close to π. The profile of $\Phi_k^G(t)$ looks quite different as compared to the non-Hermitian zero-temperature case. The winding number shows steplike jumps at the above critical times. Since $z_{n,k}$ encloses a closed loop by crossing the imaginary axis twice, the winding number is expected to exhibit both an increase and a decrease with time. However, we only find a decrease in the winding number within $3 < t < 5$, where $z_{n,k}$ crosses the real axis once.

B. Quench within horizontal gapless phase IV

We now focus on the occurrences of MSDQPT following the quench inside the gapless phase IV as shown in Fig. 1(b). Figure 3(a) depicts the lines of Fisher zeros $z_{n,k}$ crossing an imaginary axis twice for all values of n. This is in contrast to the previous situation for the quench inside the gapped phase I, presented in Fig. 2, where MSDQPT only takes place for $n > n_{\min}$. The nonanalyticities (discontinuous change) in the rate function $I(t)$ (geometric phase) are captured at the critical times $t_c \approx 1.38, 3.78, 4.71, 5.68, \ldots$ in Fig. 3(b) [3(c)]. The nonanalyticities in the rate function are more clearly visible in

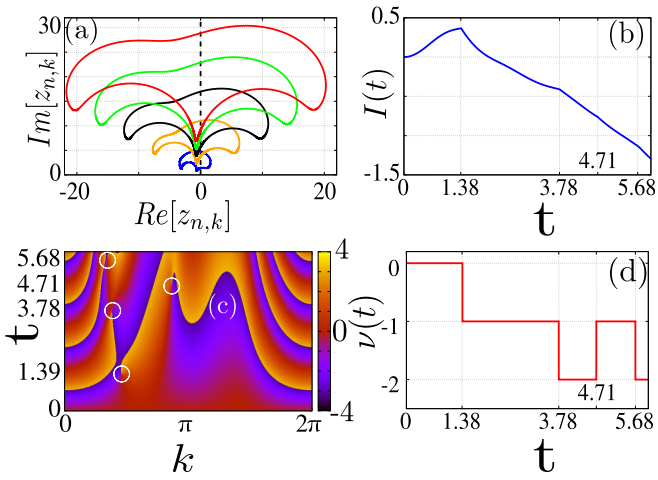

FIG. 3. We repeat Fig. 2 for the case discussed in Sec. IV B. The lines of Fisher zeros $z_{n,k}$ with $n = 0$ (blue), ..., $n = 4$ (red) cross an imaginary axis twice leading to the nonanalyticities in the rate function at critical times, $t_c \approx 1.38, 3.78, 4.71, 5.68, \ldots$, around which the winding number exhibits integer jumps. The parameters are taken to be $(\mu_i, \mu_f, \Delta_i, \Delta_f) = (0.1, 0.7, 0.2, 0.2)$.

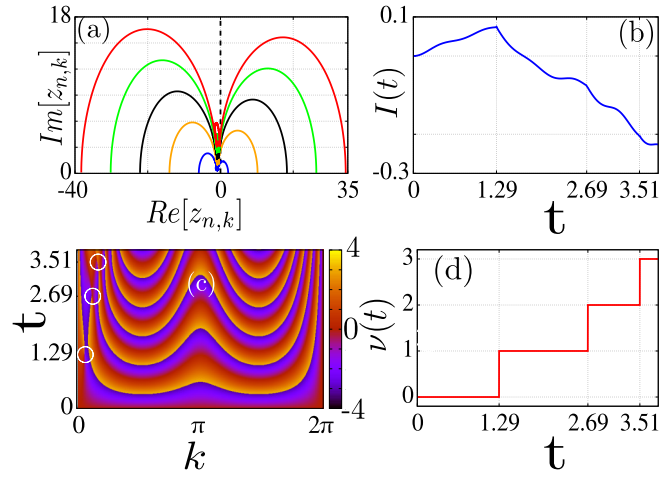

FIG. 4. We repeat Fig. 2 for the case discussed in Sec. IV C. The lines of Fisher zeros $z_{n,k}$ with $n = 0$ (blue), ..., $n = 4$ (red) cross an imaginary axis once leading to the nonanalyticities in the rate function at critical times, $t_c \approx 1.29, 2.69, 3.51, \ldots$, around which the winding number exhibits monotonic integer jumps. All the parameters are taken to be $(\mu_i, \mu_f, \Delta_i, \Delta_f) = (-1.7, -1.1, 2.2, 2.2)$.

the present case as compared to the previous one in Fig. 2(b). The winding number shows a nonmonotonic jump profile with time that is caused by the double crossing of imaginary axis by $z_{n,k}$. The important point to note here is that these jumps are always of unit magnitudes unlike the previous zero-temperature case [67]. The unit jumps are a consequence of the continuous crossing of Fisher zeros through the imaginary axis that we find in the present case.

C. Quench within vertical gapless phase V

We now demonstrate the MSDQPT following the quench within the vertical gapless phase V as presented in Fig. 1(b). Unlike the previous cases, we find here that $z_{n,k}$ crosses the imaginary axis once [see Fig. 4(a)]. The nonanalyticities in the rate function are captured with time in Fig. 4(b). The geometric phase, shown in Fig. 4(c), exhibits a similar profile as compared to that of the gapped phase I. The oscillatory profile of the geometric phase is a common characteristic of the finite-temperature case. The winding number shows a monotonic increase with time due to the single crossing of the imaginary axis by $z_{n,k}$. The unit jumps in MSDQPT, associated with finite temperature, are in contrast to the half-integer jumps of DQPT corresponding to the zero-temperature case [67]. We additionally check for the $\phi = 0$ case, where we also do not find the half-integer jumps in the winding number (not shown here).

D. Distinct temperature profile of MSDQPTs for phases I, IV, and V

As illustrated above, the MSDQPT takes place in all three phases irrespective of their gap structure. To be precise, for a given quench amplitude and temperature, there exist multiple critical times t_c's. We focus here on the evolution of the minimum critical time, referred to as $t_{\rm cm}$, that captures the minimum time taken by the system to witness the first occurrence of MSDQPT. We numerically study the temperature dependence of $t_{\rm cm}$ such that phases I, IV, and V can be distinguished.

Figures 5(a), 5(b) and 5(c) depict the temperature profile of $t_{\rm cm}$ following the large (small) intraphase quench amplitude, denoted by red (blue) lines, within regions I, IV, and V, respectively. The infinite-temperature $\beta \to 0$ value of $t_{\rm cm}$ is found to be insensitive to the quench amplitude. This suggests that MSDQPT is present anyway in the infinite-temperature case as long as the quench amplitude is finite. Connecting with Fig. 2(a), one can find that $n_{\rm min}$ increases for a smaller quench amplitude. For phase V, MSDQPT takes place early as compared to phases I and IV in the infinite-temperature limit. On the other hand, $t_{\rm cm}$ saturates with increasing β above a certain value. We now find that the zero-temperature $\beta \to \infty$ value of $t_{\rm cm}$ depends strongly on the quench amplitude [see the insets of Figs. 5(a), 5(b) and 5(c)]. To be precise, MSDQPT appears quickly with time in the zero-temperature limit for a larger quench amplitude. Interestingly, for the present case, MSDQPT occurs more quickly with time for gapless phases IV and V as compared to the gapped phase I in the limit $\beta \to \infty$.

For the intermediate temperature with a finite value of β, we find nonmonotonic behavior of $t_{\rm cm}$ only for the gapless phases IV and V. In the case of the gapped phase I as shown in Fig. 5(a), $t_{\rm cm}$ increases almost monotonically from $\beta \to 0$. This is followed by a saturation for $\beta \to \infty$. However, there exists a small dip around $\beta \approx 0$. The non-Hermiticity-induced vertical gapless phase V shows a sharp dip for intermediate values of β, while a broadened dip is noticed for complex hopping-induced horizontal gapless phase IV [Figs. 5(b) and 5(c)]. Such a dip in $t_{\rm cm}$ for gapless phases refers to the fact that MSDQPT can even appear early with time as compared to the infinite-temperature case. This is in contrast to the behavior of the gapped phase where MSDQPT can only appear at a later time for any finite temperature as compared to the

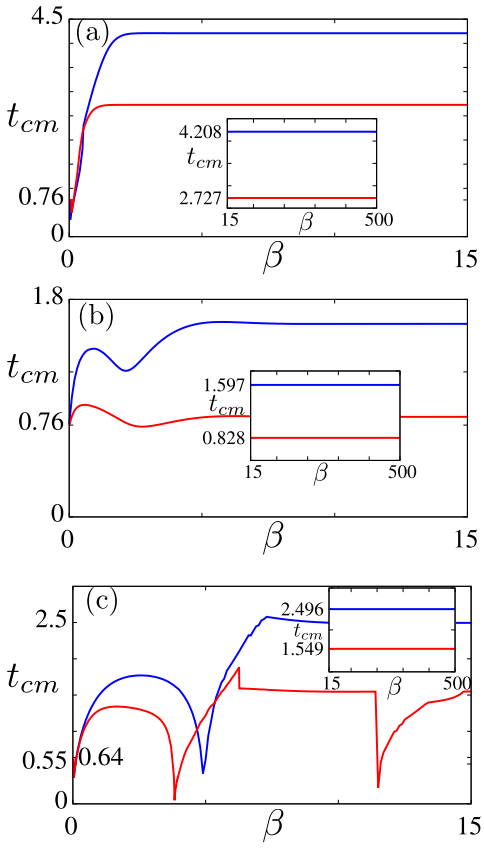

FIG. 5. We plot the minimum time $t_{\rm cm}$ required for MSDQPT to take place as a function of inverse temperature β for quench within phases I, IV, and V in (a), (b), and (c), respectively. For (a), the red (blue) line corresponds to quench path $(\mu_i,\ \mu_f,\ \Delta_i,\ \Delta_f) = (-0.7, 0.7, 2.2, 2.2)$ $[(0.1, 0.7, 2.2, 2.2)]$. For (b), the red (blue) line corresponds to quench path $(\mu_i,\ \mu_f,\ \Delta_i,\ \Delta_f) = (-0.7, 0.7, 0.2, 0.2)$ $[(0.1, 0.7, 0.2, 0.2)]$. For (c), the red (blue) line corresponds to quench path $(\mu_i,\ \mu_f,\ \Delta_i,\ \Delta_f) = (-1.7, -1.1, 2.2, 2.2)$ $[(-1.8, -1.5, 2.2, 2.2)]$. The nonmonotonic behavior in (b) and (c) is in complete contrast to that of (a). We show the saturation of $t_{\rm cm}$ over a wide range of $\beta \gg 1$ as the insets. The insets show the saturation profile of $t_{\rm cm}$ for $\beta \gg 1$. We consider $w_0 = 1$, $\phi = \pi/4$, $\gamma_1 = 0$, and $\gamma_2 = 1$.

infinite-temperature limit. The details of the dip structure of $t_{\rm cm}$ are expected to depend on the quench amplitudes for a given gapless phase. The location of such dips might depend on the details of the gapless phase, i.e., whether it is caused by non-Hermiticity or the phase of complex hopping for the identical quench amplitude. For example, the relative locations of such dips on the β axis are altered between phases IV and V. However, we emphasize that the detailed future analysis of $t_{\rm cm}$ versus β behavior is yet to be required to comment on their phase-dependent distinct characteristics.

The spectral gap profiles in phases I, IV, and V differ from each other significantly. The above analysis on MSDQPT by varying β is able to capture the interplay between the temperature and the gap profile of the eigenstates associated with these phases (see Appendix F). In the gapless regions IV and V with finite T, the minimum time $t_{\rm cm}$ at which the first destructive interference takes place is relatively less than that for gapped region I. This can be intimately connected to the distinct spectral profiles of these phases.

E. Discussion

The estimation of critical momenta, obtained from Eq. (3), is hard as far as a closed form is concerned. In the non-Hermitian case, one can use a non-Bloch form of momentum to explain the topological properties [96–100]. We can use the same non-Bloch notion to qualitatively predict the critical momenta k_c using the DQPT framework for a Hermitian system. The above effective approach is unable to predict the exact values of the critical momenta; however, one obtains a closed-form expression of k_c (see Appendix G). Importantly, it can explain the emergence of multiple k_c's, which is consistently visible for non-Hermitian cases [67]. The multivalued nature of k_c also exists for a Hermitian system. However, this nature persists more strongly as the non-Hermiticity allows for additional solutions for k_c as evident from Eq. (3).

Having demonstrated the results for quenching inside phases I, IV, and V extensively, we comment that MSDQPT is also present for quench inside phases II as well as III. Therefore, all the intraphase quench leads to MSDQPT in finite temperature when the non-Hermiticity is associated with the superconductivity. By contrast, the DQPT is not always present for all of the above cases at zero temperature [67]. On the other hand, for any interphase quench, the MSDQPT is present, but we do not show it here explicitly. The emergence of the DQPT is not intrinsically connected with the crossing of QCP and EP for Hermitian and non-Hermitian systems, respectively [63,67] at zero temperature. As shown above, the DQPT is always present as long as the critical momenta k_c exist. For the finite-temperature case, obtaining the critical momenta is even more probable due to the presence of the thermal density matrix instead of the pure quantum state. The finite-temperature broadening of the quantum energy levels yields further scope to interact with neighboring energy levels in addition to the non-Hermiticity. This might lead to the rapid variation of geometric phases for different momentum modes at a given time. As a result, one can expect to see MSDQPT for all the cases. However, we find an exception when we study the intraphase III quench in the presence of a non-Hermitian chemical potential only at finite temperature (see Appendix H). We emphasize that the half-integer jumps in the winding number for zero temperature are rounded off by the finite temperature, where the Fisher zeros do not show any discontinuity over the imaginary axis.

The temperature profiles of MSDQPT in the different phases clearly signal the distinct characteristics of the postquench evolution of a mixed quantum state (see Fig. 5). The unitary evolution of a pure quantum state results in a revival with time, referring to the fact that there exist quantum interferences between the initial and time-evolved state [101,102]. The nonanalytic divergences in the rate functions are connected with the complete destructive interferences. The absence of such interferences results in the disappearance of the DQPT. The evolution of mixed-state LA shows qualitatively similar features as far as the constructive and destructive interferences are concerned while compared with the pure state LA. However, temperature smoothes the

interference patterns, and the destructive interferences is sustained [82,103,104]. In our case, the fact that MSDQPT is always present means that complete destructive interferences are bound to happen postquench out of the mixed quantum state. For the non-Hermitian case, due to the presence of EPs, the destructive interferences are more probable [55]. As a result, the nonunitary evolution of the mixed state at finite temperature deviates from the initial configuration more often than the zero-temperature unitary counterpart. This can be connected to the thermal behavior of interacting systems where the driven systems traverse the entire phase space. Our findings on the occurrence of MSDQPT essentially refer to the fact that the non-Hermitian system might not localize in the phase space as opposed to the integrable Hermitian system leading to the finite-temperature thermal phase. A detailed investigation will be required in the future to study these aspects of DQPTs.

We now discuss the possible experimental connection as far as the model and MSDQPT are concerned. We know the p-wave superconductor is naturally unavailable, but it can be engineered using the proximity effect in Rashba nanowire with s-wave superconductivity [105]. On the other hand, the non-Hermiticity is more easily realizable in metamaterials as compared to the solid-state systems. The non-Hermitian dynamics in ultracold atoms are theoretically proposed to obtain a new regime of quantum critical phenomena [93,106,107]. The PT-symmetric dimerized photonic lattice are experimentally engineered to study the non-Hermitian topological systems [74]. Moving onto the experimental detection of MSDQPT, we can comment that the geometric phase for the mixed state can be captured by using NMR spectroscopy [108]. The DQPT for fermionic many-body states has also been experimentally captured following time-resolved state tomography in a system of ultracold atoms in optical lattices [70]. The quantum logic gates in optical lattices [109], where the NMR technique can be blended with ultracold atoms, might be instrumental in probing MSDQPT such that the geometric phase is measured for a time-evolved mixed state on a Bloch sphere. In short, we believe that a metamaterial perspective of quantum phenomena could be realized in the future to test the theoretical findings. However, predicting an exact experimental setup is beyond the scope of the present manuscript.

V. CONCLUSIONS

Considering a p-wave superconductor with complex hopping and non-Hermiticity (see Fig. 1), we examine the occurrences of MSDQPT in various gapped and gapless phases. We find that MSDQPT always exists irrespective of the gap profile of the underlying phases as long as the temperature is nonzero (see Figs. 2–4). The phase boundaries are modified by the particular choice of $\gamma_{1,2}$ in the non-Hermitian case; however, the qualitative findings on whether the MSDQPT appears remain unaltered. This is in contrast to the absence of DQPT in the gapped phases at zero temperature. The half-integer jumps of the winding number in zero temperature for the gapless phase are washed away at finite temperature. However, in the gapped phase with finite temperature, there exists a notion of a minimum integer number above which the Fisher zeros cross the imaginary axis. We do not find any such finite integer number for Fisher zeros under finite temperature in the case of gapless phases. We analyze the minimum time $t_{\rm cm}$ required by the system to experience MSDQPT as a function of the inverse temperature β such that we can distinguish the above phases (see Fig. 5). The nonmonotonic (monotonic) nature of $t_{\rm cm}$ with β is noticed for gapless (gapped) phases. There exist finer details in the behavior of $t_{\rm cm}$ with regard to the quench amplitudes through which non-Hermiticity-induced and complex-hopping-induced gapless phases can be differentiated. Our study can successfully bridge between the zero- and infinite-temperature limits. We provide an effective theoretical framework to qualitatively understand the occurrences of MSDQPT. However, we stress that the exact closed-form expression of the critical time for any finite-temperature MSDQPT is yet to be examined as a future study. For the effect of long-range hopping, various types of disorder can be studied in this context of MSDQPT. With the experimental advancement on lossy systems [71–76], we believe that the present study is experimentally viable.

ACKNOWLEDGMENTS

D.M. acknowledges SAMKHYA: High-Performance Computing Facility provided by Institute of Physics, Bhubaneswar, for numerical computations. We thank Arijit Saha for useful discussions.

APPENDIX A: INITIAL DENSITY MATRIX

The initial Hamiltonian is given by

$$H_{k,i} = \mathbf{h}_{k,i} \cdot \boldsymbol{\sigma} = h_{k,i}\hat{h}_{k,i} \cdot \vec{\sigma}. \tag{A1}$$

For temperature $T = \beta^{-1}$, using Eq. (A1) the initial ($t = 0$) density matrix is given by

$$\begin{aligned}
\rho_k(0) &= \frac{e^{-\beta H_{k,i}}}{\mathrm{Tr}[e^{-\beta H_{k,i}}]} \\
&= \frac{e^{-\beta h_{k,i}\hat{h}_{k,i}\cdot\vec{\sigma}}}{\mathrm{Tr}[e^{-\beta h_{k,i}\hat{h}_{k,i}\cdot\vec{\sigma}}]} \\
&= \frac{\cosh(\beta h_{k,i})\sigma_0 - (\hat{h}_{k,i}\cdot\vec{\sigma})\sinh(\beta h_{k,i})}{\mathrm{Tr}[\cosh(\beta h_{k,i})\sigma_0 - (\hat{h}_{k,i}\cdot\vec{\sigma})\sinh(\beta h_{k,i})]} \\
&= \frac{\cosh(\beta h_{k,i})\sigma_0 - (\hat{h}_{k,i}\cdot\vec{\sigma})\sinh(\beta h_{k,i})}{2\cosh(\beta h_{k,i})} \\
&= \tfrac{1}{2}(\sigma_0 - \tanh(\beta h_{k,i})(\hat{h}_{k,i}\cdot\vec{\sigma})) \\
&= \tfrac{1}{2}(\sigma_0 - m(\hat{h}_{k,i}\cdot\vec{\sigma})),
\end{aligned} \tag{A2}$$

where σ_0 is a 2×2 identity matrix, $m = \tanh(\beta h_{k,i})$, and $h_{k,i} = \sqrt{(h^x_{k,i})^2 + (h^y_{k,i})^2 + (h^z_{k,i})^2}$. For a Hermitian Hamiltonian, $h_{k,i}$ is the positive eigenvalue of $H_{k,i}$ that is always real. On the other hand, for a non-Hermitian Hamiltonian, the eigenvalue can be imaginary as well and $h_{k,i}$ corresponds to a positive real part of the energy eigenvalue.

Infinite temperature with the $T \to \infty$ limit, i.e., $\beta \to 0$, leads to $m = 0$. This results in

$$\rho_k(0)|_{T\to\infty} = \tfrac{1}{2}\sigma_0. \tag{A3}$$

The above expression exactly matches previous studies on the DQPT with an infinite-temperature mixed density matrix at initial time [64].

APPENDIX B: LOSCHMIDT AMPLITUDE

The final Hamiltonian is given by

$$H_{k,f} = \mathbf{h}_{k,f} \cdot \boldsymbol{\sigma} = h_{k,f}\hat{h}_{k,f} \cdot \vec{\sigma}, \tag{B1}$$

where $h_{k,f}$ represents the positive real part of the energy eigenvalue for a final Hamiltonian without loss of generality. The initial thermal density matrix is evolved with the final Hamiltonian $H_{k,f}$ in time following the sudden quench from $H_{k,i}$. The time evolution operator is given by

$$U_k(t) = e^{-iH_{k,f}t}. \tag{B2}$$

The LA at zero temperature is given by $g_k(t) = \langle\Psi_{k,i}|e^{-iH_{k,f}t}|\Psi_{k,i}\rangle = \mathrm{Tr}\,[|\Psi_{k,i}\rangle\langle\Psi_{k,i}|e^{-iH_{k,f}t}]$, where the initial pure quantum state $|\Psi_{k,i}\rangle$, associated with $H_{k,i}$, is evolved with $H_{k,f}$. In the case of finite temperature, the LA thus can be written with the initial thermal density matrix [Eq. (A2)] and time evolution operator [Eq. (B2)] as follows [10]:

$$\begin{aligned} g_k(t) &= \mathrm{Tr}[\rho_k(0)U_k(t)] \\ &= \mathrm{Tr}\left[\tfrac{1}{2}(\sigma_0 - m(\hat{h}_{k,i}\cdot\vec{\sigma}))e^{-iH_{k,f}t}\right] \\ &= \mathrm{Tr}\left[\tfrac{1}{2}(\sigma_0 - m(\hat{h}_{k,i}\cdot\vec{\sigma}))(\cos(h_{k,f}t)\right. \\ &\quad \left. - i(\hat{h}_{k,f}\cdot\vec{\sigma})\sin(h_{k,f}t))\right] \\ &= \cos(h_{k,f}t) + i\, m(\hat{h}_{k,i}\cdot\hat{h}_{k,f})\sin(h_{k,f}t) \\ &= \cos(h_{k,f}t) - i\ \sin(h_{k,f}t)B_k, \end{aligned} \tag{B3}$$

where $B_k = -m\frac{\vec{h}_{k,i}\cdot\vec{h}_{k,f}}{h_{k,i}h_{k,f}}$.

Note that in DQPT, LA plays the same role as the partition function for an equilibrium phase transition. For the infinite-temperature case with $T \to \infty$, β vanishes yielding $m = 0$. This leads to the following:

$$g_k(t)|_{T\to\infty} = \cos(h_{k,f}t). \tag{B4}$$

The above expression exactly matches with previous studies on MSDQPT [64].

APPENDIX C: LINES OF FISHER ZEROS

Similar to the vanishing of the partition function in the equilibrium phase transition, here also the lines of Fisher zeros are given by the suppression of LA, i.e., $g_k(t) = 0$. This represents a complete destructive interference between the initial and time-evolved states. From Eq. (B3), one can obtain the Fisher zeros as follows:

$$\begin{aligned} &\cos(h_{k,f}t) - i\ \sin(h_{k,f}t)B_k = 0 \\ &\Rightarrow -i\cot(h_{k,f}t) = B_k \\ &\Rightarrow \coth(ih_{k,f}t) = B_k \\ &\Rightarrow \coth(h_{k,f}z) = B_k \\ &\Rightarrow z = \frac{1}{h_{k,f}}\coth^{-1}(B_k) \\ &\Rightarrow z = \frac{1}{h_{k,f}}\times\frac{1}{2}\ln\left(\frac{B_k+1}{B_k-1}\right) \\ &\Rightarrow z = \frac{1}{2h_{k,f}}\ln(-1) + \frac{1}{2h_{k,f}}\ln\left(\frac{1+B_k}{1-B_k}\right). \end{aligned} \tag{C1}$$

Hence the general expression for Fisher zeros $z_{n,k}$ is given by

$$\begin{aligned} z_{n,k} &= i\left(n+\frac{1}{2}\right)\frac{\pi}{h_{k,f}} + \frac{1}{2h_{k,f}}\ln\left(\frac{1+B_k}{1-B_k}\right), \\ \Rightarrow z_{n,k} &= i\left(n+\frac{1}{2}\right)\frac{\pi}{h_{k,f}} + \frac{1}{h_{k,f}}\tanh^{-1}(B_k), \end{aligned} \tag{C2}$$

where $z_{n,k} = it$, and $n \in Z$. Note that $z_{n,k}$ in Eq. (C2) is a complex function, and MSDQPT happens when the lines of Fisher zeros cut the imaginary axis, i.e., $\mathrm{Re}[z_{n,k}] = 0$. This refers to the fact that $\tanh^{-1}(B_k)/h_{k,f} = 0$ with $B_k = 0$.

We again compare with the infinite-temperature case, i.e., the $T \to \infty$ limit. Here, β becomes zero giving rise to $m = 0$, $B_k = 0$. As a result, we find

$$z_{n,k}|_{T\to\infty} = i\left(n+\frac{1}{2}\right)\frac{\pi}{h_{k,f}}. \tag{C3}$$

Note that the above expression exactly matches with the previous findings [64].

APPENDIX D: CRITICAL MOMENTA

Let us define a new quantity as $C_k = \tanh^{-1}(B_k)$. Hence Eq. (C2) becomes

$$\begin{aligned} z_{n,k} &= i\left(n+\frac{1}{2}\right)\frac{\pi}{h_{k,f}} + \frac{1}{h_{k,f}}C_k \\ &= i\left(n+\frac{1}{2}\right)\pi\frac{\mathrm{Re}[h_{k,f}] - i\,\mathrm{Im}[h_{k,f}]}{|h_{k,f}|^2} \\ &\quad + \frac{\mathrm{Re}[h_{k,f}] - i\,\mathrm{Im}[h_{k,f}]}{|h_{k,f}|^2}(\mathrm{Re}[C_k] + i\,\mathrm{Im}[C_k]). \end{aligned}$$

The critical momenta k_c is then obtained by solving the equation below for k_c,

$$\begin{aligned} &\mathrm{Re}[z_{n,k_c}] = 0 \\ &\quad\Rightarrow \pi(n+1/2)\,\mathrm{Im}[h_{k_c,f}] + \mathrm{Re}[h_{k_c,f}]\,\mathrm{Re}[C_{k_c}] \\ &\qquad + \mathrm{Im}[h_{k_c,f}]\,\mathrm{Im}[C_{k_c}] = 0. \end{aligned} \tag{D1}$$

We now reduce the above expression in the case of infinite temperature. For the $T \to \infty$ limit, i.e., $\beta \to 0$, one can obtain $B_k = 0$ and $C_k = 0$. As a result, Eq. (D1) takes the

following form:

$$\mathrm{Im}[h_{k_c,f}] = 0. \tag{D2}$$

This is consistent with the previous findings [64]. We would like to point out an important observation here for γ_2, $\Delta \neq 0$ and $\gamma_1 = 0$. The above Eq. (D2) can only yield $k_c = n\pi$ with $n = 0, 1, 2, \ldots$ as the valid solution. This further indicates that the critical momenta k_c are independent of all the model parameters. To derive the above solution, we use $z^{1/2} = |z|^{1/4}\exp(i\phi/2)$ with $z = x + iy$, $\phi = \arctan(y/x)$. A complete calculation suggests that $y = 0$ is the only solution possible provided $|z| \neq 0$.

APPENDIX E: CRITICAL TIME

We derive here the critical time $t_c = -iz_{n,k_c}$ corresponding to k_c as given below,

$$t_c = \pi\left(n + \frac{1}{2}\right)\frac{\mathrm{Re}[h_{k_c,f}]}{|h_{k_c,f}|^2} + \frac{\mathrm{Re}[h_{k_c,f}]\,\mathrm{Im}[C_{k_c}] - \mathrm{Im}[h_{k_c,f}]\,\mathrm{Re}[C_{k_c}]}{|h_{k_c,f}|^2}. \tag{E1}$$

The above general expression in the case of infinite temperature can be reduced further. Considering $T \to \infty$, $\beta \to 0$, i.e., $B_k = 0$, i.e., $C_k = 0$, we find

$$t_c|_{T\to\infty} = \left(n + \frac{1}{2}\right)\frac{\pi}{\mathrm{Re}[h_{k_c,f}]}. \tag{E2}$$

This is consistent with the previous findings [64]. Using the above lines of argument, discussed after Eq. (D2), one can find that for a fixed μ_f and γ_2, $\Delta \neq 0$, $t_{\mathrm{cm}}|_{T\to\infty}$ is independent of quench amplitude. Interestingly, $t_{\mathrm{cm}}|_{T\to\infty}$ can only depend on μ_f, while the Δ dependence is completely absent for the critical momentum $k_c = n\pi$.

APPENDIX F: DYNAMICAL PHASE

The dynamical phase is merely the phase acquired by a quantum state due to the time evolution of the underlying Hamiltonian. We illustrate here the dynamical phase for the non-Hermitian system such that $H^\dagger \neq H$ [64]. Let us denote the right and left eigenvectors as $|\psi_s^r(k)\rangle$ and $|\psi_s^l(k)\rangle$, respectively. Here $s = \pm$ denotes two energy bands for the two-level systems. These eigenvectors satisfy the following equations:

$$H(k)\,|\psi_s^r(k)\rangle = E_s(k)\,|\psi_s^r(k)\rangle\,, \tag{F1}$$

$$H^\dagger(k)\,|\psi_s^l(k)\rangle = E_s^*(k)\,|\psi_s^l(k)\rangle\,. \tag{F2}$$

In this representation, the Hamiltonian H_k can be expressed as

$$H_k = \sum_{s=\pm} E_s(k)\,|\psi_s^r(k)\rangle\,\langle\psi_s^l(k)|\,. \tag{F3}$$

In the space of these left and right eigenvectors, right and left time evolution operators can be expressed as

$$U_k^r(t) = \sum_{s=\pm} e^{-iE_s(k)t}\,|\psi_s^r(k)\rangle\,\langle\psi_s^l(k)|\,, \tag{F4}$$

$$U_k^l(t) = \sum_{s=\pm} e^{-iE_s(k)t}\,|\psi_s^l(k)\rangle\,\langle\psi_s^r(k)|\,, \tag{F5}$$

respectively. The biorthogonality conditions $\sum_s |\psi_s^r(k)\rangle\langle\psi_s^l(k)| = \sigma_0$ and $\langle\psi_s^l(k)|\psi_{s'}^r(k)\rangle = \delta_{ss'}$ are required to further simplify the expressions. The time-evolved density matrix is written as $\rho_k(t) = U_k^{l\dagger}(t)\rho_k(0)U_k^r(t)$. The dynamical phase is expressed as follows [10]:

$$\begin{aligned}\Phi_k^{\mathrm{dyn}}(t) &= -\int_0^t dt'\,\mathrm{Re}\left[\frac{\mathrm{Tr}[\rho_k(t)H_{k,f}]}{\mathrm{Tr}\,[\rho_k(t)]}\right] \\ &= -\int_0^t dt'\,\mathrm{Re}\left[\frac{\mathrm{Tr}\big[U_k^{l\dagger}(t')\rho_k(0)U_k^r(t')H_{k,f}\big]}{\mathrm{Tr}\left[U_k^{l\dagger}(t')\rho_k(0)U_k^r(t')\right]}\right].\end{aligned} \tag{F6}$$

Now, using Eq. (A2), we obtain

$$\begin{aligned}\Phi_k^{\mathrm{dyn}}(t) &= -\int_0^t dt'\,\mathrm{Re}\left[\frac{\mathrm{Tr}\left[U_k^{l\dagger}(t')\times\frac{1}{2}(\sigma_0 - m(\hat{h}_{k,i}\cdot\vec{\sigma}))\times U_k^r(t')H_{k,f}\right]}{\mathrm{Tr}\left[U_k^{l\dagger}(t')\times\frac{1}{2}(\sigma_0 - m(\hat{h}_{k,i}\cdot\vec{\sigma}))\times U_k^r(t')\right]}\right] \\ &= -\int_0^t dt'\,\mathrm{Re}\left[\frac{\mathrm{Tr}\left[U_k^{l\dagger}(t')\times\frac{1}{2}\left(\sigma_0 - \frac{mH_{k,i}}{h_{k,i}}\right)\times U_k^r(t')H_{k,f}\right]}{\mathrm{Tr}\left[U_k^{l\dagger}(t')\times\frac{1}{2}\left(\sigma_0 - \frac{mH_{k,i}}{h_{k,i}}\right)\times U_k^r(t')\right]}\right].\end{aligned} \tag{F7}$$

Now using Eqs. (F3), (F4), and (F5),

$$\begin{aligned}&\mathrm{Tr}\left[U_k^{l\dagger}(t')\sigma_0 U_k^r(t')H_{k,f}\right] \\ &= \mathrm{Tr}\left[U_k^{l\dagger}(t')U_k^r(t')H_{k,f}\right] \\ &= \mathrm{Tr}\left[\sum_{s,s',s''=\pm} e^{iE_{s,f}^*(k)t'}e^{-iE_{s',f}(k)t'}E_{s'',f}(k)\times\left|\psi_{s,f}^r(k)\right\rangle\left\langle\psi_{s,f}^l(k)\right|\times\left|\psi_{s',f}^r(k)\right\rangle\left\langle\psi_{s',f}^l(k)\right|\times\left|\psi_{s'',f}^r(k)\right\rangle\left\langle\psi_{s'',f}^l(k)\right|\right]\end{aligned}$$

$$
\begin{aligned}
&= \mathrm{Tr}\left[\sum_{s,s',s''=\pm} e^{iE^*_{s,f}(k)t'} e^{-iE_{s',f}(k)t'} E_{s'',f}(k) \times \left|\psi^r_{s,f}(k)\right\rangle \left\langle\psi^l_{s'',f}(k)\right| \ \delta_{ss'}\ \delta_{s's''}\right] \\
&= \mathrm{Tr}\left[\sum_{s=\pm} e^{iE^*_{s,f}(k)t'} e^{-iE_{s,f}(k)t'} E_{s,f}(k) \times \left|\psi^r_{s,f}(k)\right\rangle \left\langle\psi^l_{s,f}(k)\right|\right] \\
&= \mathrm{Tr}\left[\sum_{s=\pm} e^{2\,\mathrm{Im}[E_{s,f}(k)]\ t'} E_{s,f}(k) \times \left|\psi^r_{s,f}(k)\right\rangle \left\langle\psi^l_{s,f}(k)\right|\right] \\
&= e^{2\,\mathrm{Im}[h_{k,f}]\ t'} h_{k,f} - e^{-2\,\mathrm{Im}[h_{k,f}]\ t'} h_{k,f} \\
&= 2\, h_{k,f} \sinh(2\,\mathrm{Im}[h_{k,f}]\, t'). \qquad \text{(F8)}
\end{aligned}
$$

Similarly,

$$\mathrm{Tr}\left[U^{l\dagger}_k(t') H_{k,i} U^r_k(t') H_{k,f}\right] = 2\, h_{k,i}\, h_{k,f} \cosh(2\,\mathrm{Im}[h_{k,f}]\, t'), \qquad \text{(F9)}$$

$$\mathrm{Tr}\left[U^{l\dagger}_k(t') \sigma_0 U^r_k(t')\right] = 2\, \cosh(2\,\mathrm{Im}[h_{k,f}]\, t'), \qquad \text{(F10)}$$

$$\mathrm{Tr}\left[U^{l\dagger}_k(t') H_{k,i} U^r_k(t')\right] = 2\, h_{k,i}\, \sinh(2\ \mathrm{Im}[h_{k,f}]\, t'). \qquad \text{(F11)}$$

Now combining all the above expressions, the dynamical phase for the non-Hermitian system is found to be

$$
\begin{aligned}
\Phi^{\mathrm{dyn}}_k(t) \ &= -\int_0^t dt'\, \mathrm{Re}\left[h_{k,f} \frac{\sinh(2\,\mathrm{Im}[h_{k,f}]\, t') - m\, \cosh(2\,\mathrm{Im}[h_{k,f}]\, t')}{\cosh(2\,\mathrm{Im}[h_{k,f}]\, t') - m\, \sinh(2\,\mathrm{Im}[h_{k,f}]\, t')}\right] \\
&= -\int_0^t dt'\, \mathrm{Re}\left[h_{k,f} \frac{\tanh(2\,\mathrm{Im}[h_{k,f}]\, t') - m}{1 - m\, \tanh(2\,\mathrm{Im}[h_{k,f}]\, t')}\right]. \qquad \text{(F12)}
\end{aligned}
$$

In the infinite-temperature $T \to \infty$ limit, the dynamical phase reads

$$\Phi^{\mathrm{dyn}}_k(t)|_{T\to\infty} = -\int_0^t dt'\, \mathrm{Re}[h_{k,f}\ \tanh(2\,\mathrm{Im}[h_{k,f}]\, t')]. \qquad \text{(F13)}$$

The above expression is consistent with earlier findings [64].

APPENDIX G: EFFECTIVE THEORY FOR NON-HERMITIAN DQPT

We discuss here the effective theory for the MSDQPT. We rewrite the non-Hermitian Hamiltonian under consideration,

$$\mathcal{H}_k(0, \gamma_2, \phi) \ = \left(2\Delta \sin k + \frac{i\gamma_2}{2}\right)\sigma_y - (2w_0 \cos\phi \cos k + \mu)\sigma_z. \qquad \text{(G1)}$$

Replacing k by $k + i\kappa$, and saying $e^{k+i\kappa} \equiv x$, we can write the above Hamiltonian as

$$\mathcal{H}_k(0, \gamma_2, \phi) \ = \left(-i\Delta(x - x^{-1}) + \frac{i\gamma_2}{2}\right)\sigma_y - (w_0 \cos\phi\ (x + x^{-1}) + \mu)\sigma_z = \mathbf{h}_k \cdot \boldsymbol{\sigma}. \qquad \text{(G2)}$$

The eigenvalues are given by

$$E_\pm = \pm\sqrt{\left(-i\Delta(x - x^{-1}) + \frac{i\gamma_2}{2}\right)^2 + (w_0 \cos\phi\ (x + x^{-1}) + \mu)^2}. \qquad \text{(G3)}$$

Now, in the $E_\pm \to 0$ limit, we get

$$-\left(-\Delta(x^2 - 1) + \frac{\gamma_2}{2}x\right)^2 + (w_0 \cos\phi\ (x^2 + 1) + \mu x)^2 = 0. \qquad \text{(G4)}$$

Solutions of the above equation are

$$x_1 = \frac{\frac{\gamma_2}{2} - \mu - \sqrt{\left(\mu - \frac{\gamma_2}{2}\right)^2 - 4(w_0 \cos\phi - \Delta)(\Delta + w_0 \cos\phi)}}{2(\Delta + w_0 \cos\phi)},$$

$$x_2 = \frac{\frac{\gamma_2}{2} - \mu + \sqrt{\left(\mu - \frac{\gamma_2}{2}\right)^2 - 4(w_0 \cos\phi - \Delta)(\Delta + w_0 \cos\phi)}}{2(\Delta + w_0 \cos\phi)},$$

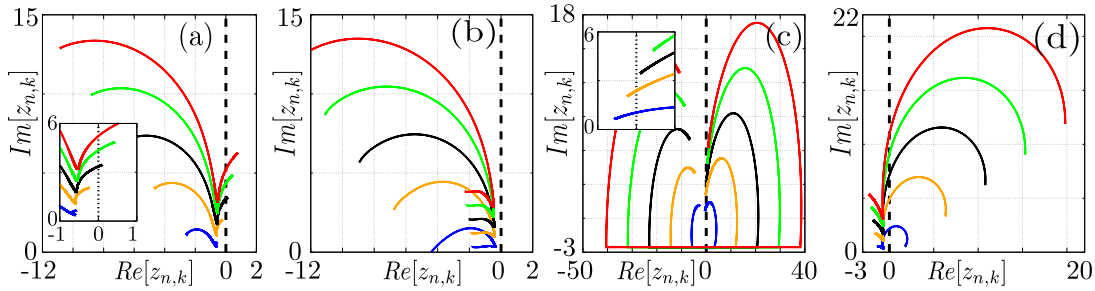

FIG. 6. The lines of Fisher zeros are plotted with $n = 0$ (blue), ..., $n = 4$ (red) for the cases of non-Hermitian chemical potential with ($\gamma_1 = 1, \gamma_2 = 0$). The Fisher zeros for the quench within gapped phase I, III are shown in (a) for (μ_i, μ_f, Δ_i, Δ_f) = (0.1, 0.7, 2.2, 2.2) and in (b) for (μ_i, μ_f, Δ_i, Δ_f) = (−4.7, −2.1, 2.2, 2.2), respectively. The same is shown for gapless phases IV and V in (c) for (μ_i, μ_f, Δ_i, Δ_f) = (0.1, 0.7, 0.2, 0.2) and in (d) for (μ_i, μ_f, Δ_i, Δ_f) = (−1.7, −1.1, 2.2, 2.2), respectively. We find that there exists $n_{\min} = 1$ in (a) above which the Fisher zeros cross the imaginary axis referring to the occurrence of MSDQPT. The lines of Fisher zeros do not cross the imaginary axis for any value of n, indicating the absence of MSDQPT in (b). There exists an $n_{\max} = 1$ above which the Fisher zeros do not cross the imaginary axis referring to the fact that MSDQPT can only be observed for short times in (c). The lines of Fisher zeros always cross the imaginary axis, confirming the occurrences of MSDQPT in (d). We consider ($w_0, \phi, \gamma_1, \gamma_2, \beta$) = (1, $\frac{\pi}{4}$, 1, 0, 1).

$$x_3 = \frac{\frac{\gamma_2}{2} + \mu - \sqrt{\frac{\gamma_2^2}{4} + \gamma_2\,\mu + 4\Delta^2 + \mu^2 - 2w_0^2\cos 2\phi - 2w_0^2}}{2(\Delta - w_0\cos\phi)},$$

$$x_4 = \frac{\frac{\gamma_2}{2} + \mu + \sqrt{\frac{\gamma_2^2}{4} + \gamma_2\,\mu + 4\Delta^2 + \mu^2 - 2w_0^2\cos 2\phi - 2w_0^2}}{2(\Delta - w_0\cos\phi)}. \tag{G5}$$

Now, $x_1x_2x_3x_4 = 1$, $x_1x_2 = \frac{-\Delta+w_0\cos\phi}{\Delta+w_0\cos\phi}$, and $x_3x_4 = \frac{\Delta+w_0\cos\phi}{-\Delta+w_0\cos\phi}$. Therefore, x can be written as $x = (x_1x_2x_3x_4)^{1/4}$, or $x = \sqrt{x_1x_2}$, or $x = \sqrt{x_3x_4}$, however none of the above is a good choice as their final expressions are independent of γ_2. We hence use $x = \sqrt{x_1x_4}$ as it depends on γ_2. This allows us to write Eq. (G2) as follows:

$$h_k^y = -i\Delta(e^{ik}x - e^{-ik}x^{-1}) + \frac{i\gamma_2}{2}, \tag{G6}$$

$$h_k^z = -[w_0\cos\phi\ (e^{ik}x + e^{-ik}x^{-1}) + \mu]. \tag{G7}$$

To get the critical momentum, k_c, we use the known DQPT framework for the Hermitian system using $\vec{h}_{k_c,i}\cdot\vec{h}_{k_c,f}$ [10] for our case such that

$$h_{k_c,i}^y h_{k_c,f}^y + h_{k_c,i}^z h_{k_c,f}^z = 0. \tag{G8}$$

Solving the above equation for a fixed quench amplitude, one can get multiple critical momenta k_c unlike single critical momentum for the Hermitian case [10]. This can qualitatively explain the emergence of multiple k_c's for the non-Hermitian case.

APPENDIX H: MISSING MSDQPT FOR NON-HERMITIAN CHEMICAL POTENTIAL

We consider here the non-Hermiticity only in the chemical potential, i.e., $\gamma_1 = 1$ and $\gamma_2 = 0$. Note that the phase diagram changes for the lossy chemical potential, however the phases I, II, III, IV, and V are present similar to the lossy superconductivity (see Fig. 1). We study the behavior of the Fisher zeros for quench within the phases I, III, IV, and V, as shown in Figs. 6(a), 6(b), 6(c), and 6(d), respectively. We find that MSDQPT can exist for phases I, IV, and V except for phase III as the Fisher zeros cross the imaginary axis in the prior phases but not in the later phase. This is in contrast to the non-Hermitian superconductor case in which the MSDQPT always persists irrespective of the phases as long as the temperature is nonzero. On the other hand, for phases I and IV, one can find $n_{\min}$ and $n_{\max}$, respectively, for the lines of Fisher zeros, indicating that MSDQPT is absent below (above) a certain timescale. This timescale is directly related to $n_{\min}$ and $n_{\max}$ for phases I and IV, respectively. For the case of a non-Hermitian superconductor, we do not find any such $n_{\max}$ in phase IV, however we do find $n_{\min}$ for phase I. Therefore, the gapped and gapless phases for the non-Hermitian superconductor and the non-Hermitian chemical potential do not show identical properties as far as the MSDQPT is concerned. Interestingly, for quench within region III, we find the absence of MSDQPT for the finite-temperature non-Hermitian chemical potential similar to the zero-temperature case [67]. However, likewise the zero-temperature case, we do not find any discontinuity in the Fisher zeros in any of the above cases.

APPENDIX I: MSDQPT IN THE HERMITIAN LIMIT

In this Appendix, we concentrate on the Hermitian limit of our system, i.e., $\gamma_1 = \gamma_2 = 0$. The phase diagram is different

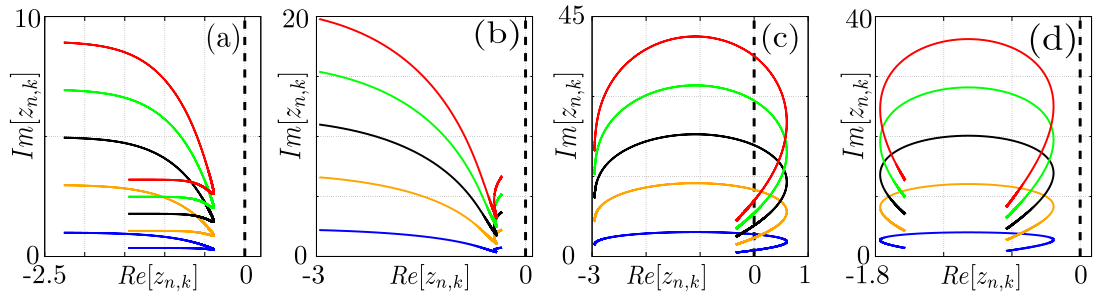

FIG. 7. The lines of Fisher zeros are depicted with $n = 0$ (blue), …, $n = 4$ (red) for the Hermitian case ($\gamma_1 = 0, \gamma_2 = 0$). The Fisher zeros for the quench within gapped phases III, and I are shown in (a) for $(\mu_i, \mu_f, \Delta_i, \Delta_f) = (-5, -3, 2.2, 2.2)$ and in (b) for $(\mu_i, \mu_f, \Delta_i, \Delta_f) = (-0.7, 0.7, 2.2, 2.2)$, respectively. Clearly, there is no crossing over the imaginary axis, which confirms the absence of MSDQPT. We do the same for two different quench metrics within the gapless phase IV in (c) for $(\mu_i, \mu_f, \Delta_i, \Delta_f) = (-0.7, 0.7, 0.2, 0.2)$ and in (d) for $(\mu_i, \mu_f, \Delta_i, \Delta_f) = (-0.3, 0.7, 0.2, 0.2)$, respectively. Here, the lines of Fisher zeros cross (do not cross) the imaginary axis twice in (c) [(d)], suggesting the occurrence of MSDQPT (absence of MSDQPT) with two types of k_c. We choose $(w_0, \phi, \beta) = (1, \frac{\pi}{4}, 1)$.

for the Hermitian case as compared to the non-Hermitian counterpart. The vertical gapless region V vanishes completely, while the horizontal gapless region IV vanishes (becomes narrower) for $\phi = 0$ ($\phi = \pi/4$). We are interested in $\phi = \pi/4$ here as it supports an extended gapless region where we can observe its effects on MSDQPT following an intraphase quench. One can rewrite the expressions for the physical quantities such as the rate function, Fisher zeros, and dynamical phases in the Hermitian limit. Note that for the Hermitian case, energy eigenvalues are real, i.e., $\mathrm{Im}[h_{k,i}] = \mathrm{Im}[h_{k,f}] = 0$, suggesting B_k in Eqs. (B3) and (C2) are real. This does not result in any change in the expression for LA, $g_k(t)$, lines of Fisher zeros, $z_{n,k}$, and total phase, $\Phi_k^{\mathrm{tot}}(t)$, while the critical momenta is obtained from

$$\vec{h}_{k_c,i} \cdot \vec{h}_{k_c,f} = 0. \tag{I1}$$

The critical time is found to be

$$t_c = \left(n + \frac{1}{2}\right) \frac{\pi}{h_{k_c,f}}. \tag{I2}$$

However, the dynamical phase has a simple form as

$$\Phi_k^{\mathrm{dyn}}(t) = -\int_0^t dt' m h_{k,f} = -m h_{k,f} t. \tag{I3}$$

Here, we are interested only in the lines of Fisher zeros that are enough to confirm the occurrences of MSDQPT. We investigate the Fisher zero profiles for quenches within regions III and I, which are shown in Figs. 7(a) and 7(b), respectively. The noncrossing nature conveys the absence of the MSDQPT for an intraphase quench inside region I. Therefore, for intraphase quench within region I, Fig. 7(b), suggests that MSDQPT does not happen. By contrast, $(\gamma_1, \gamma_2) = (\neq 0, 0)$ and $(0, \neq 0)$ as shown in Figs. 6(a) and 4, respectively, and we find that MSDQPT exists, which is a marked difference as compared to the finite-temperature Hermitian case. The MSDQPT is absent for the intraphase quench in region III irrespective of the Hermiticity of the problem [see Figs. 7(a) and 6(b)]. The Fisher zeros are depicted in Fig. 7(c) [7(d)] for a large (short) quench metric within region IV. Interestingly, the lines of Fisher zeros cross an imaginary axis twice indicating MSDQPT for two types of critical momenta in Fig. 7(c). On the other hand, the lines of Fisher zeros do not cross the imaginary axis referring to the absence of MSDQPT as demonstrated in Fig. 7(d). Based on the above analysis on the Hermitian case at finite temperature ($\beta = 1$), we can comment that the results are similar as obtained for the zero-temperature case [67].

[1] M. E. Fisher, The theory of equilibrium critical phenomena, Rep. Prog. Phys. **30**, 615 (1967).

[2] C. N. Yang and T. D. Lee, Statistical theory of equations of state and phase transitions. I. Theory of condensation, Phys. Rev. **87**, 404 (1952).

[3] T. D. Lee and C. N. Yang, Statistical theory of equations of state and phase transitions. II. Lattice gas and ising model, Phys. Rev. **87**, 410 (1952).

[4] M. Heyl, A. Polkovnikov, and S. Kehrein, Dynamical Quantum Phase Transitions in the Transverse-Field Ising Model, Phys. Rev. Lett. **110**, 135704 (2013).

[5] J. N. Kriel, C. Karrasch, and S. Kehrein, Dynamical quantum phase transitions in the axial next-nearest-neighbor ising chain, Phys. Rev. B **90**, 125106 (2014).

[6] C. Karrasch and D. Schuricht, Dynamical phase transitions after quenches in nonintegrable models, Phys. Rev. B **87**, 195104 (2013).

[7] M. Heyl, Scaling and Universality at Dynamical Quantum Phase Transitions, Phys. Rev. Lett. **115**, 140602 (2015).

[8] M. Heyl, Dynamical quantum phase transitions: A review, Rep. Prog. Phys. **81**, 054001 (2018).

[9] E. Canovi, P. Werner, and M. Eckstein, First-Order Dynamical Phase Transitions, Phys. Rev. Lett. **113**, 265702 (2014).

[10] U. Bhattacharya, S. Bandyopadhyay, and A. Dutta, Mixed state dynamical quantum phase transitions, Phys. Rev. B **96**, 180303(R) (2017).

[11] R. Jafari, H. Johannesson, A. Langari, and M. A. Martin-Delgado, Quench dynamics and zero-energy modes: The case of the creutz model, Phys. Rev. B **99**, 054302 (2019).
[12] S. Vajna and B. Dóra, Disentangling dynamical phase transitions from equilibrium phase transitions, Phys. Rev. B **89**, 161105(R) (2014).
[13] S. Vajna and B. Dóra, Topological classification of dynamical phase transitions, Phys. Rev. B **91**, 155127 (2015).
[14] A. Khatun and S. M. Bhattacharjee, Boundaries and Unphysical Fixed Points in Dynamical Quantum Phase Transitions, Phys. Rev. Lett. **123**, 160603 (2019).
[15] T. Nag, Excess energy and decoherence factor of a qubit coupled to a one-dimensional periodically driven spin chain, Phys. Rev. E **93**, 062119 (2016).
[16] S. Suzuki, T. Nag, and A. Dutta, Dynamics of decoherence: Universal scaling of the decoherence factor, Phys. Rev. A **93**, 012112 (2016).
[17] R. Sachdeva, T. Nag, A. Agarwal, and A. Dutta, Finite-time interaction quench in a luttinger liquid, Phys. Rev. B **90**, 045421 (2014).
[18] T. Nag, U. Divakaran, and A. Dutta, Scaling of the decoherence factor of a qubit coupled to a spin chain driven across quantum critical points, Phys. Rev. B **86**, 020401(R) (2012).
[19] H. T. Quan, Z. Song, X. F. Liu, P. Zanardi, and C. P. Sun, Decay of Loschmidt Echo Enhanced by Quantum Criticality, Phys. Rev. Lett. **96**, 140604 (2006).
[20] F. M. Cucchietti, D. A. R. Dalvit, J. P. Paz, and W. H. Zurek, Decoherence and the Loschmidt Echo, Phys. Rev. Lett. **91**, 210403 (2003).
[21] R. Jafari and H. Johannesson, Loschmidt Echo Revivals: Critical and Noncritical, Phys. Rev. Lett. **118**, 015701 (2017).
[22] P. Uhrich, N. Defenu, R. Jafari, and J. C. Halimeh, Out-of-equilibrium phase diagram of long-range superconductors, Phys. Rev. B **101**, 245148 (2020).
[23] M. Schmitt and S. Kehrein, Dynamical quantum phase transitions in the kitaev honeycomb model, Phys. Rev. B **92**, 075114 (2015).
[24] J. C. Halimeh and V. Zauner-Stauber, Dynamical phase diagram of quantum spin chains with long-range interactions, Phys. Rev. B **96**, 134427 (2017).
[25] B. Žunkovič, M. Heyl, M. Knap, and A. Silva, Dynamical Quantum Phase Transitions in Spin Chains with Long-Range Interactions: Merging Different Concepts of Nonequilibrium Criticality, Phys. Rev. Lett. **120**, 130601 (2018).
[26] J. C. Halimeh, M. Van Damme, V. Zauner-Stauber, and L. Vanderstraeten, Quasiparticle origin of dynamical quantum phase transitions, Phys. Rev. Res. **2**, 033111 (2020).
[27] T. Hashizume, I. P. McCulloch, and J. C. Halimeh, Dynamical phase transitions in the two-dimensional transverse-field ising model, Phys. Rev. Res. **4**, 013250 (2022).
[28] J. Lang, B. Frank, and J. C. Halimeh, Concurrence of dynamical phase transitions at finite temperature in the fully connected transverse-field ising model, Phys. Rev. B **97**, 174401 (2018).
[29] I. Homrighausen, N. O. Abeling, V. Zauner-Stauber, and J. C. Halimeh, Anomalous dynamical phase in quantum spin chains with long-range interactions, Phys. Rev. B **96**, 104436 (2017).
[30] L. Rossi and F. Dolcini, Nonlinear current and dynamical quantum phase transitions in the flux-quenched su-schrieffer-heeger model, Phys. Rev. B **106**, 045410 (2022).
[31] U. Mishra, R. Jafari, and A. Akbari, Disordered kitaev chain with long-range pairing: Loschmidt echo revivals and dynamical phase transitions, J. Phys. A **53**, 375301 (2020).
[32] U. Divakaran, S. Sharma, and A. Dutta, Tuning the presence of dynamical phase transitions in a generalized *xy* spin chain, Phys. Rev. E **93**, 052133 (2016).
[33] S. Sharma, U. Divakaran, A. Polkovnikov, and A. Dutta, Slow quenches in a quantum ising chain: Dynamical phase transitions and topology, Phys. Rev. B **93**, 144306 (2016).
[34] S. Sharma, S. Suzuki, and A. Dutta, Quenches and dynamical phase transitions in a nonintegrable quantum ising model, Phys. Rev. B **92**, 104306 (2015).
[35] A. Dutta and A. Dutta, Probing the role of long-range interactions in the dynamics of a long-range kitaev chain, Phys. Rev. B **96**, 125113 (2017).
[36] S. Zamani, R. Jafari, and A. Langari, Floquet dynamical quantum phase transition in the extended xy model: Nonadiabatic to adiabatic topological transition, Phys. Rev. B **102**, 144306 (2020).
[37] R. Jafari and A. Akbari, Floquet dynamical phase transition and entanglement spectrum, Phys. Rev. A **103**, 012204 (2021).
[38] R. Jafari, A. Akbari, U. Mishra, and H. Johannesson, Floquet dynamical quantum phase transitions under synchronized periodic driving, Phys. Rev. B **105**, 094311 (2022).
[39] J. Naji, R. Jafari, L. Zhou, and A. Langari, Engineering floquet dynamical quantum phase transitions, Phys. Rev. B **106**, 094314 (2022).
[40] K. Yang, L. Zhou, W. Ma, X. Kong, P. Wang, X. Qin, X. Rong, Y. Wang, F. Shi, J. Gong, and J. Du, Floquet dynamical quantum phase transitions, Phys. Rev. B **100**, 085308 (2019).
[41] L. Zhou and Q. Du, Floquet dynamical quantum phase transitions in periodically quenched systems, J. Phys.: Condens. Matter **33**, 345403 (2021).
[42] T. Palmai, Edge exponents in work statistics out of equilibrium and dynamical phase transitions from scattering theory in one-dimensional gapped systems, Phys. Rev. B **92**, 235433 (2015).
[43] F. Andraschko and J. Sirker, Dynamical quantum phase transitions and the loschmidt echo: A transfer matrix approach, Phys. Rev. B **89**, 125120 (2014).
[44] R. Modak and D. Rakshit, Many-body dynamical phase transition in a quasiperiodic potential, Phys. Rev. B **103**, 224310 (2021).
[45] M. Abdi, Dynamical quantum phase transition in bose-einstein condensates, Phys. Rev. B **100**, 184310 (2019).
[46] M. Syed, T. Enss, and N. Defenu, Dynamical quantum phase transition in a bosonic system with long-range interactions, Phys. Rev. B **103**, 064306 (2021).
[47] S. Stumper, M. Thoss, and J. Okamoto, Interaction-driven dynamical quantum phase transitions in a strongly correlated bosonic system, Phys. Rev. Res. **4**, 013002 (2022).
[48] A. Kosior, A. Syrwid, and K. Sacha, Dynamical quantum phase transitions in systems with broken continuous time and space translation symmetries, Phys. Rev. A **98**, 023612 (2018).
[49] A. Kosior and K. Sacha, Dynamical quantum phase transitions in discrete time crystals, Phys. Rev. A **97**, 053621 (2018).
[50] E. J. Bergholtz and J. C. Budich, Non-Hermitian weyl physics in topological insulator ferromagnet junctions, Phys. Rev. Res. **1**, 012003(R) (2019).

[51] K. Yang, S. C. Morampudi, and E. J. Bergholtz, Exceptional Spin Liquids from Couplings to the Environment, Phys. Rev. Lett. **126**, 077201 (2021).

[52] V. Kozii and L. Fu, Non-Hermitian topological theory of finite-lifetime quasiparticles: prediction of bulk fermi arc due to exceptional point, arXiv:1708.05841.

[53] T. Yoshida, R. Peters, and N. Kawakami, Non-Hermitian perspective of the band structure in heavy-fermion systems, Phys. Rev. B **98**, 035141 (2018).

[54] H. Shen, B. Zhen, and L. Fu, Topological Band Theory for Non-Hermitian Hamiltonians, Phys. Rev. Lett. **120**, 146402 (2018).

[55] E. J. Bergholtz, J. C. Budich, and F. K. Kunst, Exceptional topology of non-Hermitian systems, Rev. Mod. Phys. **93**, 015005 (2021).

[56] A. Ghatak and T. Das, New topological invariants in non-Hermitian systems, J. Phys.: Condens. Matter **31**, 263001 (2019).

[57] Y. Ashida, Z. Gong, and M. Ueda, Non-Hermitian physics, Adv. Phys. **69**, 249 (2020).

[58] K. Kawabata, K. Shiozaki, M. Ueda, and M. Sato, Symmetry and Topology in Non-Hermitian Physics, Phys. Rev. X **9**, 041015 (2019).

[59] T. Yoshida, T. Mizoguchi, and Y. Hatsugai, Mirror skin effect and its electric circuit simulation, Phys. Rev. Res. **2**, 022062(R) (2020).

[60] T. Yoshida, R. Peters, N. Kawakami, and Y. Hatsugai, Symmetry-protected exceptional rings in two-dimensional correlated systems with chiral symmetry, Phys. Rev. B **99**, 121101(R) (2019).

[61] T. Yoshida, Real-space dynamical mean field theory study of non-Hermitian skin effect for correlated systems: Analysis based on pseudospectrum, Phys. Rev. B **103**, 125145 (2021).

[62] J. C. Budich and M. Heyl, Dynamical topological order parameters far from equilibrium, Phys. Rev. B **93**, 085416 (2016).

[63] L. Zhou, Q.-H. Wang, H. Wang, and J. Gong, Dynamical quantum phase transitions in non-Hermitian lattices, Phys. Rev. A **98**, 022129 (2018).

[64] L. Zhou and Q. Du, Non-hermitian topological phases and dynamical quantum phase transitions: a generic connection, New J. Phys. **23**, 063041 (2021).

[65] J. Naji, M. Jafari, R. Jafari, and A. Akbari, Dissipative floquet dynamical quantum phase transition, Phys. Rev. A **105**, 022220 (2022).

[66] R. Hamazaki, Exceptional dynamical quantum phase transitions in periodically driven systems, Nat. Commun. **12**, 5108 (2021).

[67] D. Mondal and T. Nag, Anomaly in the dynamical quantum phase transition in a non-Hermitian system with extended gapless phases, Phys. Rev. B **106**, 054308 (2022).

[68] P. Jurcevic, H. Shen, P. Hauke, C. Maier, T. Brydges, C. Hempel, B. P. Lanyon, M. Heyl, R. Blatt, and C. F. Roos, Direct Observation of Dynamical Quantum Phase Transitions in an Interacting Many-Body System, Phys. Rev. Lett. **119**, 080501 (2017).

[69] X. Nie, B.-B. Wei, X. Chen, Z. Zhang, X. Zhao, C. Qiu, Y. Tian, Y. Ji, T. Xin, D. Lu, and J. Li, Experimental Observation of Equilibrium and Dynamical Quantum Phase Transitions via Out-of-Time-Ordered Correlators, Phys. Rev. Lett. **124**, 250601 (2020).

[70] N. Fläschner, D. Vogel, M. Tarnowski, B. Rem, D.-S. Lühmann, M. Heyl, J. Budich, L. Mathey, K. Sengstock, and C. Weitenberg, Observation of dynamical vortices after quenches in a system with topology, Nat. Phys. **14**, 265 (2018).

[71] W. Gou, T. Chen, D. Xie, T. Xiao, T.-S. Deng, B. Gadway, W. Yi, and B. Yan, Tunable Nonreciprocal Quantum Transport through a Dissipative Aharonov-Bohm Ring in Ultracold Atoms, Phys. Rev. Lett. **124**, 070402 (2020).

[72] J. Li, A. K. Harter, J. Liu, L. de Melo, Y. N. Joglekar, and L. Luo, Observation of parity-time symmetry breaking transitions in a dissipative floquet system of ultracold atoms, Nat. Commun. **10**, 855 (2019).

[73] J. M. Zeuner, M. C. Rechtsman, Y. Plotnik, Y. Lumer, S. Nolte, M. S. Rudner, M. Segev, and A. Szameit, Observation of a Topological Transition in the Bulk of a Non-Hermitian System, Phys. Rev. Lett. **115**, 040402 (2015).

[74] S. Weimann, M. Kremer, Y. Plotnik, Y. Lumer, S. Nolte, K. G. Makris, M. Segev, M. C. Rechtsman, and A. Szameit, Topologically protected bound states in photonic parity–time-symmetric crystals, Nat. Mater. **16**, 433 (2017).

[75] W. Zhu, X. Fang, D. Li, Y. Sun, Y. Li, Y. Jing, and H. Chen, Simultaneous Observation of a Topological Edge State and Exceptional Point in an Open and Non-Hermitian Acoustic System, Phys. Rev. Lett. **121**, 124501 (2018).

[76] H. Gao, H. Xue, Q. Wang, Z. Gu, T. Liu, J. Zhu, and B. Zhang, Observation of topological edge states induced solely by non-hermiticity in an acoustic crystal, Phys. Rev. B **101**, 180303(R) (2020).

[77] P. Zanardi, H. T. Quan, X. Wang, and C. P. Sun, Mixed-state fidelity and quantum criticality at finite temperature, Phys. Rev. A **75**, 032109 (2007).

[78] Y.-C. Liang, Y.-H. Yeh, P. E. Mendonça, R. Y. Teh, M. D. Reid, and P. D. Drummond, Quantum fidelity measures for mixed states, Rep. Prog. Phys. **82**, 076001 (2019).

[79] S.-J. Gu, Fidelity approach to quantum phase transitions, Int. J. Mod. Phys. B **24**, 4371 (2010).

[80] H. T. Quan and F. M. Cucchietti, Quantum fidelity and thermal phase transitions, Phys. Rev. E **79**, 031101 (2009).

[81] J. Lang, B. Frank, and J. C. Halimeh, Dynamical Quantum Phase Transitions: A Geometric Picture, Phys. Rev. Lett. **121**, 130603 (2018).

[82] B. Mera, C. Vlachou, N. Paunković, V. R. Vieira, and O. Viyuela, Dynamical phase transitions at finite temperature from fidelity and interferometric Loschmidt echo induced metrics, Phys. Rev. B **97**, 094110 (2018).

[83] S. Bandyopadhyay, S. Laha, U. Bhattacharya, and A. Dutta, Exploring the possibilities of dynamical quantum phase transitions in the presence of a Markovian bath, Sci. Rep. **8**, 11921 (2018).

[84] X.-Y. Hou, Q.-C. Gao, H. Guo, Y. He, T. Liu, and C.-C. Chien, Ubiquity of zeros of the Loschmidt amplitude for mixed states in different physical processes and its implication, Phys. Rev. B **102**, 104305 (2020).

[85] X.-Y. Hou, Q.-C. Gao, H. Guo, and C.-C. Chien, Metamorphic dynamical quantum phase transition in double-quench processes at finite temperatures, Phys. Rev. B **106**, 014301 (2022).

[86] H. Lang, Y. Chen, Q. Hong, and H. Fan, Dynamical quantum phase transition for mixed states in open systems, Phys. Rev. B **98**, 134310 (2018).

[87] N. Sedlmayr, M. Fleischhauer, and J. Sirker, Fate of dynamical phase transitions at finite temperatures and in open systems, Phys. Rev. B **97**, 045147 (2018).
[88] E. Sjöqvist, A. K. Pati, A. Ekert, J. S. Anandan, M. Ericsson, D. K. L. Oi, and V. Vedral, Geometric Phases for Mixed States in Interferometry, Phys. Rev. Lett. **85**, 2845 (2000).
[89] A. Y. Kitaev, Unpaired majorana fermions in quantum wires, Phys. Usp. **44**, 131 (2001).
[90] W. DeGottardi, D. Sen, and S. Vishveshwara, Majorana Fermions in Superconducting 1D Systems Having Periodic, Quasiperiodic, and Disordered Potentials, Phys. Rev. Lett. **110**, 146404 (2013).
[91] W. DeGottardi, M. Thakurathi, S. Vishveshwara, and D. Sen, Majorana fermions in superconducting wires: Effects of long-range hopping, broken time-reversal symmetry, and potential landscapes, Phys. Rev. B **88**, 165111 (2013).
[92] A. Rajak, T. Nag, and A. Dutta, Possibility of adiabatic transport of a majorana edge state through an extended gapless region, Phys. Rev. E **90**, 042107 (2014).
[93] Y. B. Shi and Z. Song, Topological phase in Kitaev chain with spatially separated pairing processes, Phys. Rev. B **107**, 125110 (2023).
[94] L. Li, C. H. Lee, S. Mu, and J. Gong, Critical non-Hermitian skin effect, Nat. Commun. **11**, 5491 (2020).
[95] C. Yuce, Majorana edge modes with gain and loss, Phys. Rev. A **93**, 062130 (2016).
[96] S. Yao and Z. Wang, Edge States and Topological Invariants of Non-Hermitian Systems, Phys. Rev. Lett. **121**, 086803 (2018).
[97] F. K. Kunst, E. Edvardsson, J. C. Budich, and E. J. Bergholtz, Biorthogonal Bulk-Boundary Correspondence in Non-Hermitian Systems, Phys. Rev. Lett. **121**, 026808 (2018).
[98] T. Helbig, T. Hofmann, S. Imhof, M. Abdelghany, T. Kiessling, L. W. Molenkamp, C. H. Lee, A. Szameit, M. Greiter, and R. Thomale, Generalized bulk–boundary correspondence in non-Hermitian topolectrical circuits, Nat. Phys. **16**, 747 (2020).
[99] K. Kawabata, M. Sato, and K. Shiozaki, Higher-order non-Hermitian skin effect, Phys. Rev. B **102**, 205118 (2020).
[100] A. K. Ghosh and T. Nag, Non-Hermitian higher-order topological superconductors in two dimensions: Statics and dynamics, Phys. Rev. B **106**, L140303 (2022).
[101] A. Rajak and A. Dutta, Survival probability of an edge Majorana in a one-dimensional p-wave superconducting chain under sudden quenching of parameters, Phys. Rev. E **89**, 042125 (2014).
[102] A. Rajak and T. Nag, Survival probability in a quenched Majorana chain with an impurity, Phys. Rev. E **96**, 022136 (2017).
[103] P. Cappellaro, L. Viola, and C. Ramanathan, Coherent-state transfer via highly mixed quantum spin chains, Phys. Rev. A **83**, 032304 (2011).
[104] S. Sur and V. Subrahmanyam, Loschmidt echo of local dynamical processes in integrable and non integrable spin chains, J. Phys. A **52**, 345301 (2019).
[105] A. Das, Y. Ronen, Y. Most, Y. Oreg, M. Heiblum, and H. Shtrikman, Zero-bias peaks and splitting in an al–inas nanowire topological superconductor as a signature of Majorana fermions, Nat. Phys. **8**, 887 (2012).
[106] Y. Ashida, S. Furukawa, and M. Ueda, Parity-time-symmetric quantum critical phenomena, Nat. Commun. **8**, 15791 (2017).
[107] Y. Ashida, S. Furukawa, and M. Ueda, Quantum critical behavior influenced by measurement backaction in ultracold gases, Phys. Rev. A **94**, 053615 (2016).
[108] J. Du, P. Zou, M. Shi, L. C. Kwek, J.-W. Pan, C. H. Oh, A. Ekert, D. K. L. Oi, and M. Ericsson, Observation of Geometric Phases for Mixed States using NMR Interferometry, Phys. Rev. Lett. **91**, 100403 (2003).
[109] G. K. Brennen, C. M. Caves, P. S. Jessen, and I. H. Deutsch, Quantum Logic Gates in Optical Lattices, Phys. Rev. Lett. **82**, 1060 (1999).